AGN outflows and their properties in Mrk 766 as revealed by KOOLS-IFU on the Seimei Telescope

Kyuseok Oh [1,*], **Yoshihiro Ueda** [2], **Satoshi Yamada** [3], **Yoshiki Toba** [4,5,6,†], **Keisuke Isogai** [7,8], **Atsushi Tanimoto** [9], **Shoji Ogawa** [10], **Ryosuke Uematsu** [2], **Yuya Nakatani** [2], **Kanta Fujiwara** [2], **Yuta Okada** [2], **Kazuya Matsubayashi** [11], **Kenta Setoguchi** [2]

[1]Korea Astronomy and Space Science Institute, Daedeokdae-ro 776, Yuseong-gu, Daejeon 34055, Republic of Korea
[2]Department of Astronomy, Kyoto University, Kitashirakawa-Oiwake-cho, Sakyo-ku, Kyoto 606-8502, Japan
[3]RIKEN Cluster for Pioneering Research, 2-1 Hirosawa, Wako, Saitama 351-0198, Japan
[4]National Astronomical Observatory of Japan, 2-21-1 Osawa, Mitaka, Tokyo 181-8588, Japan
[5]Academia Sinica Institute of Astronomy and Astrophysics, 11F of Astronomy-Mathematics Building, AS/NTU, No.1, Section 4, Roosevelt Road, Taipei 10617, Taiwan
[6]Research Center for Space and Cosmic Evolution, Ehime University, 2-5 Bunkyo-cho, Matsuyama, Ehime 790-8577, Japan
[7]Okayama Observatory, Kyoto University, 3037-5 Honjo, Kamogatacho, Asakuchi, Okayama 719-0232, Japan
[8]Department of Multi-Disciplinary Sciences, Graduate School of Arts and Sciences, The University of Tokyo, 3-8-1 Komaba, Meguro, Tokyo 153-8902, Japan
[9]Graduate School of Science and Engineering, Kagoshima University, Kagoshima 890-0065, Japan
[10]Institute of Space and Astronautical Science (ISAS), Japan Aerospace Exploration Agency (JAXA), 3-1-1 Yoshinodai, Chuo-ku, Sagamihara, Kanagawa 252-5210, Japan
[11]Institute of Astronomy, School of Science, The University of Tokyo 2-21-1 Osawa, Mitaka, Tokyo 181-0015, Japan
*E-mail: oh@kasi.re.kr

arXiv:2504.02936v1 [astro-ph.GA] 3 Apr 2025

Abstract

We present the emission-line flux distributions and their ratios, as well as the gas outflow features, of the innermost 2 kpc region of the type 1 Seyfert galaxy Mrk 766, using the Kyoto Okayama Optical Low-dispersion Spectrograph with an optical-fiber integral field unit on the Seimei Telescope. We find that the central region of Mrk 766 is kinematically disturbed, exhibiting asymmetric and radially distributed AGN-driven ionized gas outflows traced by [O III]λ5007 with velocities exceeding $500\ \mathrm{km\ s^{-1}}$. The mass of the ionized gas outflow is estimated to be $10^{4.65-5.95}\,M_{\odot}$, and the mass outflow rate is $0.14 - 2.73\ \mathrm{M_{\odot}\ yr^{-1}}$. This corresponds to a kinetic power, $\dot{E}_{\mathrm{K}}$, of $4.31 \times 10^{40}\ \mathrm{erg\ s^{-1}} < \dot{E}_{\mathrm{K}} < 8.62 \times 10^{41}\ \mathrm{erg\ s^{-1}}$, which is equivalent to $0.08\% - 1.53\%$ of the bolometric luminosity, L_{bol}. This result is consistent with other observed properties of ionized gas outflows, although it is lower than the theoretical predictions in AGN feedback models ($\sim 5\%$), implying that ionized gas outflows traced by [O III]λ5007 represent only a minor fraction of the total outflows ejected from the host galaxy. Given the asymmetric and radially distributed outflow signatures observed across the host galaxy within the limited field of view, the maximum distance the outflowing gas has traveled remains an open question.

Keywords: galaxies: active — galaxies: Seyfert — methods: observational

1 Introduction

Classical spectroscopic studies have been playing a critical role in investigating various properties of Active Galactic Nuclei (AGNs). Both fiber and slit spectroscopy have been used to acquire optical spectra of nearby AGNs, from which we can extract important information not only about supermassive black holes (SMBHs) and structure of AGNs but also about host galaxies (e.g., mass of SMBHs, Eddington accretion rate, metallicity, chemical enrichment, age, kinematics, and so on).

Recent advances in integral field unit (IFU) spectroscopy have opened a new era that traditional approaches could not achieve. In particular, optical IFU observations from dedicated survey such as the SDSS-IV (Blanton et al. 2017) Mapping Nearby Galaxies at APO (MaNGA, Bundy et al. (2015); Drory et al. (2015); Law et al. (2015); Yan et al. (2016)) have identified 'hidden' AGN signatures from spatially resolved regions of host galaxies (Wylezalek

et al. 2018; Mezcua & Domínguez Sánchez 2020; Cano-Díaz et al. 2022).

AGN could be displaced from the center of its host galaxy due to a recent galaxy merger (Comerford & Greene 2014; Barrows et al. 2018; Bellovary et al. 2019). Another plausible explanation is that AGN may have recently been turned off (Shapovalova et al. 2010; McElroy et al. 2016), causing light echoes to travel large distances

Table 1. Basic properties of Mrk766.*

Name	RA (J2000.0)	Dec (J2000.0)	Redshift	V mag	AGN type
(1)	(2)	(3)	(4)	(5)	(6)
Mrk 766	12:18:26.51	+29:48:46.58	0.01292423	13.6	NLS1

* Columns: (1) Object name. (2)-(3) Right ascension (RA) and declination (Dec) (J2000.0). (4) Spectroscopic redshift (Koss et al. 2022). (5) V-band magnitude (Véron-Cetty & Véron 2010). (6) AGN type (Osterbrock & Pogge 1985).

from the center and revealing their highly ionized relic signatures (Keel et al. 2012, 2015; Schawinski et al. 2015; Bland-Hawthorn et al. 2019).

By virtue of powerful capabilities of IFU observations, the ionized gas kinematics of sizable samples of AGNs has been intensely studied over the last decade. Studies have shown that kiloparsec-scale AGN-driven powerful outflows are prevalent (Liu et al. 2013b; Harrison et al. 2014; McElroy et al. 2015; Rupke et al. 2017; Deconto-Machado et al. 2022; Gatto et al. 2024) not only in the centers of host galaxies but also in their extended regions, which were difficult to explore using traditional fiber and slit spectroscopy. These gas outflows are one of the key ingredients in the framework of the Λ Cold Dark Matter (ΛCDM) cosmological model, as they regulate star formation, which is expected to align with the galaxy luminosity function. For this reason, IFU observations are essential not only for uncovering unknown and interesting features of AGNs but also as a crucial part of galaxy formation models.

The Kyoto Okayama Optical Low-dispersion Spectrograph with optical fiber IFU (KOOLS-IFU, Matsubayashi et al. (2019)) on Okayama 3.8m Seimei telescope (Kurita et al. 2020) has started its science operation since 2019. It has been actively used to explore unseen features from many fascinating Galactic (Otsuka 2022; Otsuka et al. 2023; Taguchi et al. 2023; Namekata et al. 2024) as well as extragalactic sources including AGNs (Toba et al. 2022; Hoshi et al. 2024; Nagoshi et al. 2024; Toba et al. 2024).

In this paper, we present the results of optical IFU observations of Mrk 766, one of the well-known nearby AGNs classified as a narrow-line Seyfert 1 galaxy (NLS1, Osterbrock & Pogge (1985)), conducted for the first time using the KOOLS-IFU on the Seimei telescope. This paper is organized as follows. In Section 2, we describe the data we acquired and its analysis. In Section 3, we present the results along with measured quantities and discuss our findings, including important caveats. Finally, we briefly summarize our results in Section 4. We assume a cosmology with $h = 0.70$, $\Omega_M = 0.30$, and $\Omega_\Lambda = 0.70$ throughout this work.

2 Data and analysis

2.1 Target and observations

We chose Mrk 766 (also known as NGC 4253, table 1) for this work because it has been widely studied across multiwavelength regime, from X-rays (Miller et al. 2007; Risaliti et al. 2011; Tombesi et al. 2012; Yamada et al. 2024) to near-infrared (NIR, Rodríguez-Ardila et al. (2005); Schönell et al. (2014); Riffel et al. (2023)) and radio (Kukula et al. 1995). Gonzalez Delgado & Perez (1996) reported the prominent emission lines in the optical and NIR bands using long-slit spectroscopy, indicating the presence of outflows originating from the nucleus.

Furthermore, as a part of the optical follow-up spectroscopic survey of the all-sky hard X-ray selected AGNs (Oh et al. 2018), BAT AGN Spectroscopic Survey (BASS[1], Koss et al. (2017)) presented optical emission-line properties of Mrk 766 (Oh et al. 2022) including the mass of the SMBH ($\log M_{\rm BH} = 6.82^{+0.07}_{-0.10}$ $M_\odot$, Mejía-Restrepo et al. (2022)). Earlier, Woo & Urry (2002) and Bentz et al. (2009) measured $\log M_{\rm BH}$ to be 6.54 $M_\odot$ and $6.25^{+0.28}_{-0.69}$ $M_\odot$, respectively. Given that the errors in measuring black hole mass are dominated by the intrinsic spread of virial black hole mass estimates, which is on the order of 0.5 dex, the
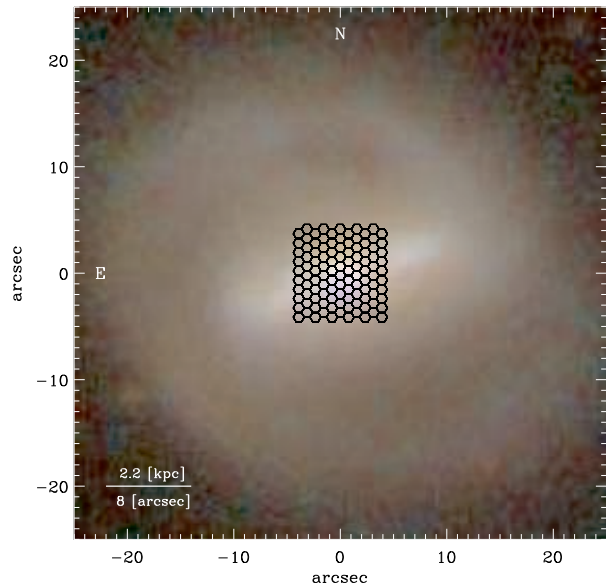

Fig. 1. SDSS *gri* color composite image of Mrk 766, overlaid with the KOOLS-IFU arrays (black hexagons, 8.4″ × 8″).

Table 2. Observation log.

Name	Date	Exp.time VPH495	Exp.time VPH683	Stardard star
Mrk 766	2024.04.13	500 × 3*	500 × 3*	HR5191

*The total integration time is 1500 sec for each grism.

reported measurements are in agreement with each other. The measurements of $\log M_{\rm BH}$ and $\log L_{\rm bol} = 43.75$ erg s^{-1} by Koss et al. (2022) yield -1.25 for $\log(L/L_{\rm Edd})$. The bolometric luminosity by Koss et al. (2022) was calculated using the X-ray $(14 - 150 \ {\rm keV})$ intrinsic luminosity (Ricci et al. (2017), $\kappa = 8$), which is equivalent to a $2 - 10$ keV with a conversion factor of 20 (Vasudevan et al. 2009) assuming $\Gamma = 1.8$.

The observational data were taken using the KOOLS-IFU instrument operating on the Seimei Telescope under the programme 24A-K-0013 (PI: Y. Ueda). The KOOLS-IFU consists of 110 fibers[2] with a total field of view (FoV) of 8.4″ by 8″, which corresponds to approximately 2 kpc × 2 kpc (figure 1). We used the VPH 495 and VPH 683 grisms which have spectral resolution of $R(= \lambda/\Delta\lambda) = 1500 - 2000$. The observation log is summarized in table 2.

2.2 Data reduction

We reduced the data using the standard reduction pipeline[3] for KOOLS-IFU, which employs the Image Reduction and Analysis Facility (IRAF, Tody (1986, 1993)). For spectrum extraction, flat-fielding, and wavelength calibration, we used the Hydra package (Barden et al. 1994; Barden & Armandroff 1995). We calibrated the wavelength using arc lamp frames (Ne and Hg). Absolute flux calibration of the spectrum was performed using standard star frames. To account for background sky levels, we took sky frames separately and subtracted them from the data frames. Considering
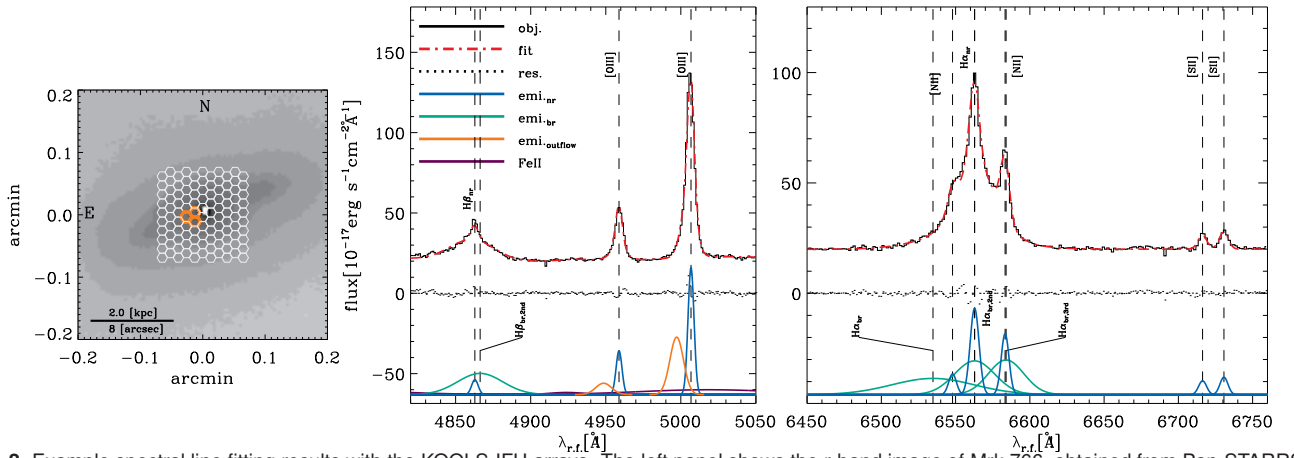

Fig. 2. Example spectral line fitting results with the KOOLS-IFU arrays. The left panel shows the r-band image of Mrk 766, obtained from Pan-STARRS1 (Chambers et al. 2016), overlaid with the KOOLS-IFU arrays. The region from which the spectrum is extracted is marked with orange hexagons. The middle and right panels present the detailed spectral fits. The black line represents the observed spectrum in the rest frame, while the red dashed-dotted line indicates the best fit. The blue Gaussians represent narrow emission-line components, and the green Gaussians represent broad emission-line components. Gas outflow components and FeII templates are depicted with orange and purple lines, respectively. The decomposed models are shown with arbitrary offsets for clarity. The dots in both panels represent the residuals.

the typical seeing at the site ($1.2'' - 1.4''$) and the field of view of each fiber, which has a regular hexagonal shape with a radius of $0.42''$, we combined data obtained from three adjacent fibers and present the results throughout this work (see left panel in Fig 2). As a result, we present data extracted from 98 out of a total of 110 fibers, of which 12 fibers located on the outskirts of the full arrays are not used.

2.3 Spectral fitting

We performed the spectral line fitting of the KOOLS-IFU data following the detailed procedures outlined by Sarzi et al. (2006) and Oh et al. (2011), which have been extensively used for various types of spectra (Oh et al. 2015, 2017; Rey et al. 2021; Oh et al. 2019, 2022). We first deredshifted the extracted spectra and corrected them for Galactic foreground extinction ($E(B - V) = 0.0197$, Schlegel et al. (1998)) using the dust attenuation curve of Calzetti et al. (2000). We fitted the stellar continuum using the penalized pixel fitting method (pPXF, Cappellari & Emsellem (2004)) which employs the stellar population models (Bruzual & Charlot 2003) and the MILES empirical stellar libraries (Sánchez-Blázquez et al. 2006). We masked regions where emission lines are expected to be present using masks with widths of 1200 km s^{-1}. When broad lines are observed in the Balmer series, wider masks are employed to accommodate at least several thousand km s^{-1} of broadening. In addition to nebular emission lines that could potentially affect continuum fitting, we masked skylines (5577Å, 6300Å, and 6363Å) as well as NaD $\lambda\lambda$5890, 5896 absorption lines during the process using the same line widths.

After fitting the stellar continuum, we used the `gandalf` code (Sarzi et al. 2006) to simultaneously match the stellar continuum and emission lines. Emission lines are modeled to be Gaussian using either single or multiple templates (e.g., Balmer lines, [O III]$\lambda\lambda$4959,5007, and [N II]$\lambda\lambda$6547,6584). We adopted the relative strengths of some emission lines based on atomic physics and the gas temperature (doublets, triplets, and Balmer lines, see table 1 in Oh et al. (2011)).

To resolve the shifts and widths of the Gaussian templates, we used the standard Levenberg-Marquardt optimization (MPFIT IDL

routine; Markwardt (2009)). The stellar line-of-sight velocity dispersions derived from the earlier step were used to broaden the stellar templates in the fit. In the presence of broad Balmer line features, we applied additional Gaussian components with a full width at half maximum (FWHM) greater than 1000 km s^{-1}. For complex broad emission features presented in the Hβ and/or Hα spectral regions, as demonstrated in the middle and right panels in figure 2, we allowed multiple Gaussian components with shifted line centers, if necessary. We measured the error of the emission-line fluxes by resampling each emission line based on the 100 realizations with randomly added noise and measuring its 1σ dispersion.

3 Results and discussion

3.1 Spatially resolved maps of derived properties

We present spatially resolved maps of derived properties within the innermost 2 kpc $\times$ 2 kpc scale covered by the KOOLS-IFU arrays. Figure 3 shows maps of the observed narrow emission-line luminosities (Hβ, [O III]λ5007, Hα, and [N II]λ6584). We did not correct for internal extinction for the sake of simplicity, as some fibers located in the outskirts exhibited poor SN ratios. This can be justified by the fact that the BPT diagram is, by definition, insensitive to dust extinction due to the small wavelength separation of the emission lines used.

In figure 4, we present a spatially resolved map of the Baldwin, Phillips, and Terlevich (BPT) diagram (Baldwin et al. 1981). We used both theoretical and empirical demarcation lines (Kewley et al. 2001; Kauffmann et al. 2003; Kewley et al. 2006; Schawinski et al. 2007) to classify regions as star-forming region (SF), composite, Seyfert, and low-ionization nuclear emission-line region (LINER). Although we employed the full classification scheme outlined above, it is noteworthy that the majority of the regions observed by the KOOLS-IFU arrays within an approximately 2 kpc $\times$ 2 kpc scale are classified as Seyfert (red filled hexagons in figure 4) according to the diagnostic diagram ([O III]λ5007/Hβ vs. [N II]λ6583/Hα), with some hexagons indicating LINERs in the outskirts.
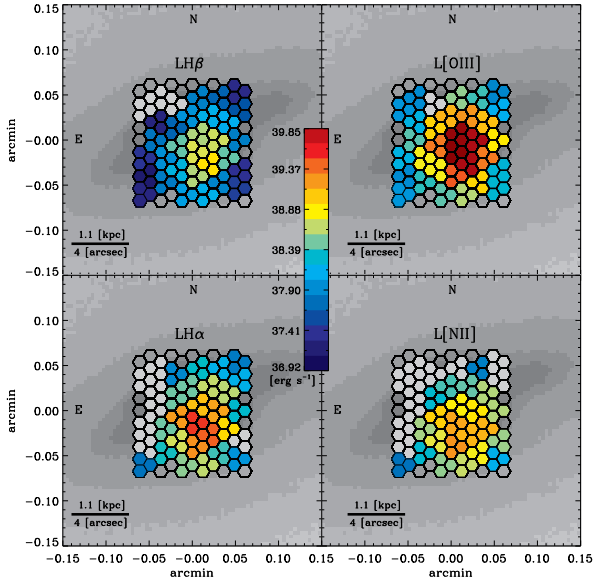
Fig. 3. Emission-line luminosities (Hβ, [O III]λ5007, [N II]λ6584, and Hα, from top-left to bottom-left in clockwise). Gray hexagons denote the KOOLS-IFU fibers for which line luminosity could not be calculated due to poor SN. Emission-line luminosities are color-coded in log scale.
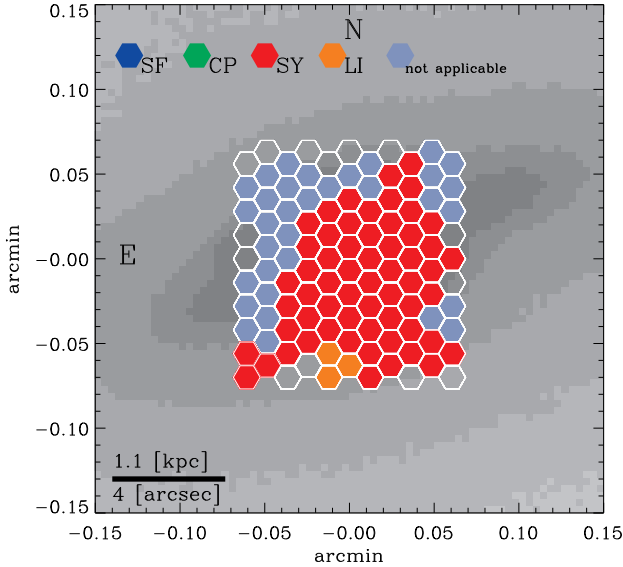

Fig. 4. Spatially resolved map of BPT diagnostics diagram ([O III]λ5007/Hβ). Blue, green, red, and orange colors are designed to denote SF, composite, Seyfert, and LINER, respectively. Light blue hexagons indicate the fibers that could not be diagnosed either due to poor SN ratio ($<$ 3) or non-detection of the given emission lines.

3.2 Non-parametric emission line measures

In order to analyze strong gas outflow emission lines detected near [O III]λ5007 (middle panel in figure 2), we exploited non-parametric emission line measures following Harrison et al. (2014) and McElroy et al. (2016). The non-parametric line width, W_{80}, which is the line width containing the central 80 per cent of the flux, is defined as follows,

$$W_{80} = v_{90} - v_{10}, \qquad (1)$$

where v_{90} and v_{10} are defined as the velocities at 90 and 10 per cent of the line flux, respectively.

An asymmetric parameter, Δv, is defined as follows,

$$\Delta v = \frac{v_{05} + v_{95}}{2} - v_{\mathrm{med}}, \qquad (2)$$

where v_{05} and v_{95} are the velocities at 5 and 95 per cent of the line flux, respectively. v_{med} is the median velocity that bisects the total flux of the emission line, allowing us to trace the direction of the propagating outflow gas across the host galaxy.

Figure 5 clearly demonstrates that the innermost 2 kpc $\times$ 2 kpc region of Mrk 766 exhibits highly disturbed ionized gas kinematics, characterized by high-velocity ($>$500 km s^{-1}, Wylezalek et al. (2020)) blue-shifted component observed in the [O III]λ5007 emission-line. An asymmetric emission-line profile, featuring a blue wing that reaches high velocities, is a definitive signature of an AGN-driven outflow (Harrison et al. 2016; Kakkad et al. 2020). Such extremely broad blue-shifted emission lines are highly unlikely to arise from normal rotational motions in galaxy kinematics (Vega Beltrán et al. 2001) or supernovae-driven outflows (Thacker et al. 2006). It should be noted that a similar, albeit larger, threshold in W_{80} ($>$600 km s^{-1}) was used in previous works studying quasars (e.g., Kakkad et al. (2020)).

The right panel in figure 5 provides insight into the distribution of outflowing gas components across the host galaxy within the observed region. It is evident that the radially distributed AGN-driven outflow gas is shaping the map of Δv in figure 5, extending in the south-east and south-west directions from the center, and is marginally misaligned with the galaxy bar.

This trend is prominent in figure 6. Notably, the AGN-driven outflow gas is not strongest at the center of galaxy, where the AGN of Mrk 766 is located. The outflow gas velocity at the center exceeds 500 km s^{-1} (orange filled hexagons and panel (c) in figure 6). The AGN-driven outflows are weaker in the north-east (panel (a)) and north-west (panel (b)) directions compared to the central region. In contrast, the strongest outflow component ($W_{80} \approx 860$ km s^{-1}) is identified in the south-west direction (panel (d)), along with a strong outflow component found at the edge of the KOOLS-IFU arrays in the south-east direction.

These AGN-driven outflows near [O III]λ5007 in a kpc-scale represent new findings in optical spectroscopy. Note that earlier work by Oh et al. (2022) demonstrated the AGN nature of Mrk 766 through emission-line diagnostics and the presence of broad Balmer features via optical long-slit spectroscopy, which lacks sufficient spectral resolution and the capability to detect outflow signatures from regions beyond the center of the host galaxy.

The detection of AGN-driven outflows on different physical scales has been reported across multiwavelength regimes, including X-rays, optical, NIR, and radio. From the analysis of X-ray data, ultrafast outflows on sub-parsec scales have been discussed (Tombesi et al. 2012; Yamada et al. 2024). Yamada et al. (2024), in particular, presented the ultrafast outflow velocities exceeding 10,000 km s^{-1}, detected over a 10-year period from 2005 to 2015. Fischer et al. (2013) noted the presence of highly blue-shifted

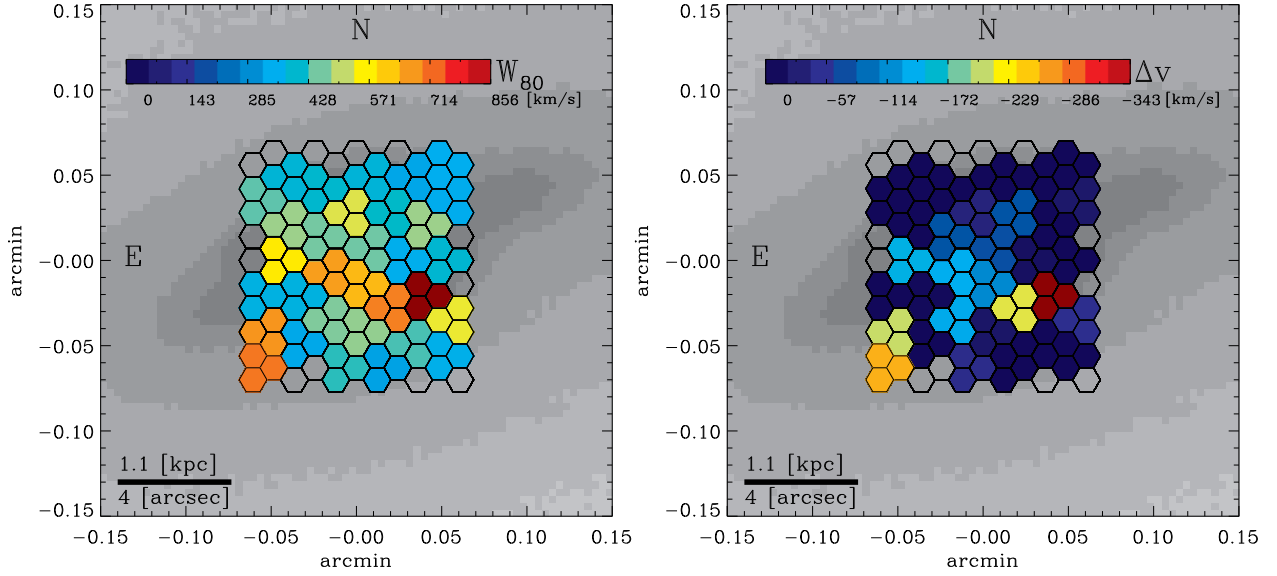**Fig. 5.** Spatially resolved map of W_{80} (left) and Δv (right). Asymmetric emission-line profiles with blue-shifted components are indicated by negative signs and color codes in the right panel.

velocity components in Mrk 766 using Hubble Space Telescope (HST) Space Telescope Imaging Spectrograph (STIS), concluding that the outflow cannot be resolved into individual components. In the NIR, Schönell et al. (2014) and Riffel et al. (2023) showed evidence of an outflow using the Near Infrared Integral Field Spectrograph (NIFS) at the Gemini Telescope. Schönell et al. (2014) concluded that the outflow is present at a position angle of approximately $135°$, which is consistent with the results of the present study, where the [FeII] velocity dispersion is increased and coincides with the location of the radio jet (Kukula et al. 1995). It is worth noting that the NIR studies using NIFS covered a smaller region of approximately $900\,\mathrm{pc} \times 900\,\mathrm{pc}$, which corresponds to about 20% of the area observed in this study.

3.3 Outflow properties

The mass of the ionized outflowing gas can be expressed as follows,

$$M_{\mathrm{out}} = 5.3 \times 10^7 \frac{L_{44}([\mathrm{OIII}])}{n_e 10^{[\mathrm{O/H}]}} M_\odot, \qquad (3)$$

where $L_{44}([\mathrm{OIII}])$ is the extinction-corrected luminosity of the outflow component detected in [OIII]$\lambda 5007$, measured in units of 10^{44} erg s^{-1}, n_e is the electron density in the outflowing gas, expressed in units of 10^3 cm^{-3}, and $10^{[\mathrm{O/H}]}$ represents the oxygen abundance in Solar units (see Appendix B in Cano-Díaz et al. (2012) for more details). Assuming the electron density to be 50 cm$^{-3} < n_e < 1000$ cm^{-3}, we find the mass of the ionized outflowing gas to be $10^{4.65} - 10^{5.95} M_\odot$. Under the same assumptions regarding the oxygen abundance and the same range for n_e, we find the mass of the ionized outflowing gas to be $10^{4.52} - 10^{5.82} M_\odot$ using the formulae from Carniani et al. (2015). The electron density derived from the [S II]$\lambda\lambda 6717, 6731$ is known to be significantly lower than that measured by several other recent methods, such as those using auroral lines and the ionization parameter. Indeed, determining the electron density is a highly uncertain and complex issue, as it varies as a function of luminosity, ionization parame-

ter, and distance from the AGN (Davies et al. 2020). Therefore, we leave the values of the ionized outflowing gas as a range that varies with the choice of n_e, rather than assuming a constant.

The mass of the ionized outflowing gas presented in this study is most likely a lower limit for two reasons. First, the limited field of view of the KOOLS-IFU instrument corresponds to approximately $2\,\mathrm{kpc} \times 2\,\mathrm{kpc}$, covering the central part of the host galaxy. We do not have additional data outside of the given FoV, which could contribute to the total ionized outflowing gas. Second, and more importantly, the ionized outflow gas traced by [O III]$\lambda 5007$ is a subset of the total outflow.

The outflow rate of ionized gas can be denoted as follows (Cano-Díaz et al. 2012),

$$\dot{M}_{\mathrm{out}} = 164 \frac{L_{44}([\mathrm{OIII}]) v}{n_e 10^{[\mathrm{O/H}]} R_{\mathrm{kpc}}} \, M_\odot \, \mathrm{yr}^{-1}, \qquad (4)$$

where v is the outflow velocity in units of 1000 km s^{-1}, and R_{kpc} is the radius of the outflowing region, in units of kpc. By adopting $v = 1000$ km s^{-1}, 50 cm$^{-3} < n_e < 1000$ cm^{-3}, and $R_{\mathrm{kpc}} = 1$ kpc for simplicity, we find the ionized gas outflow mass rate to be $0.14 - 2.73 \, M_\odot \mathrm{yr}^{-1}$.

Tombesi et al. (2012) and Riffel et al. (2023) reported $\sim 0.001 - 1 \, M_\odot \mathrm{yr}^{-1}$ and $\sim 0.3 \, M_\odot \mathrm{yr}^{-1}$ for $\dot{M}^{\mathrm{out}}$, respectively. Given the different bands (X-ray, NIR vs. optical), spectroscopic lines (Fe K, Brγ vs. [O III]$\lambda 5007$), and assumptions (fixed n_e vs. variable) used to measure $\dot{M}^{\mathrm{out}}$, it is difficult to directly compare them to each other. However, we would like to note that the inferred $\dot{M}^{\mathrm{out}}$ values are consistent within an order of magnitude.

The kinetic power of the ionized gas components of the outflows can be expressed as,

$$\dot{E}_{\mathrm{K}} = 5.17 \times 10^{43} \frac{L_{44}([\mathrm{OIII}]) v^3}{n_e 10^{[\mathrm{O/H}]} R_{\mathrm{kpc}}} \, \mathrm{erg} \, \mathrm{s}^{-1}, \qquad (5)$$

following the same assumptions and notations as adopted above. We find the kinetic power ($\dot{E}_{\mathrm{K}}$) associated with the outflows to be 4.31×10^{40} erg s$^{-1} < \dot{E}_{\mathrm{K}} < 8.62 \times 10^{41}$ erg s^{-1}. The measured $\dot{E}_{\mathrm{K}}$ corresponds to $0.08\% - 1.53\%$ of L_{bol}, under the given
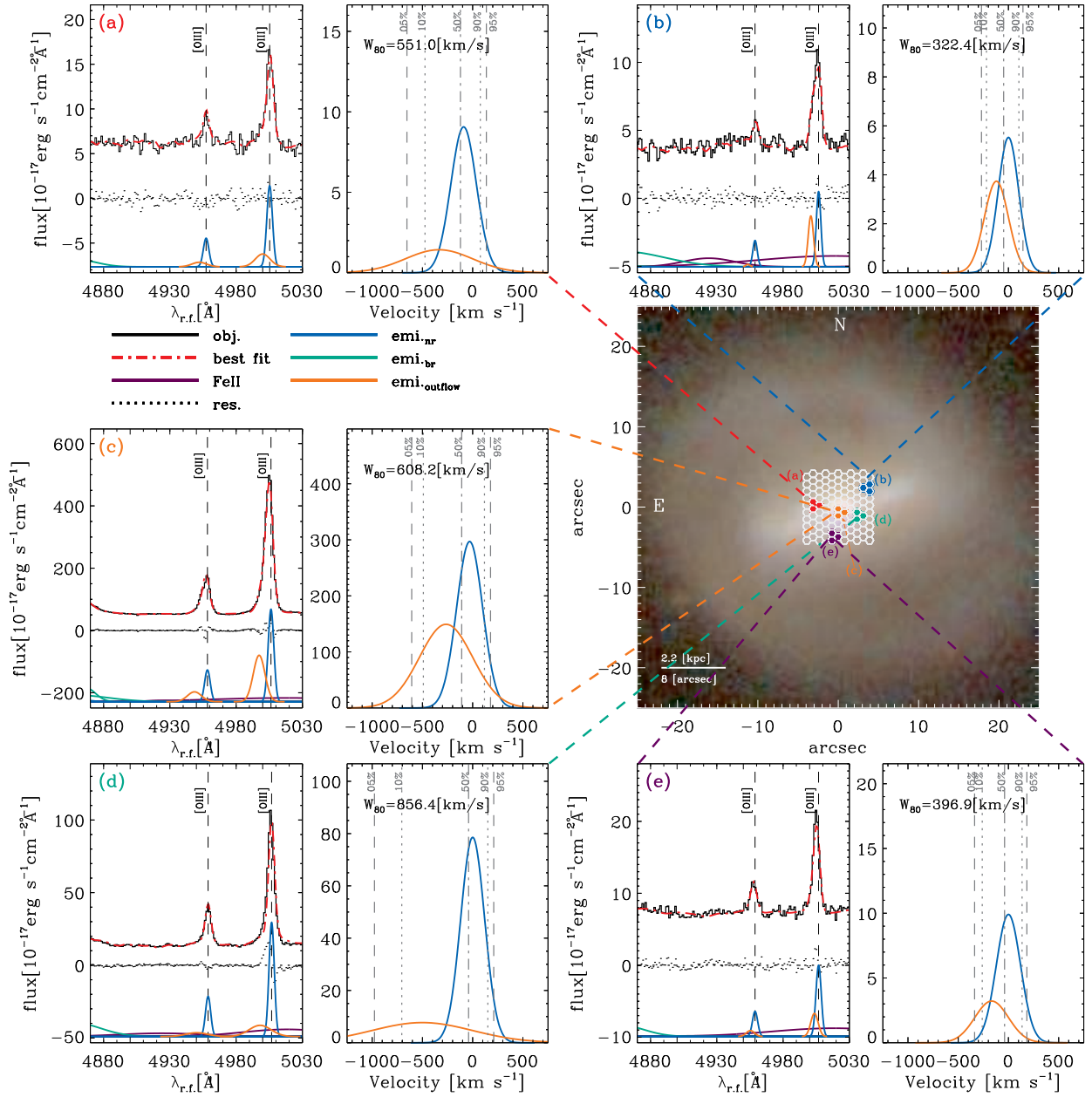
Fig. 6. AGN-driven outflow gas components detected within the KOOLS-IFU arrays across the host galaxy. The vertical dark grey lines in the panels indicating velocity denote v_{05}, v_{10}, v_{50}, v_{90}, and v_{95} (see Section 3.2). Color-filled hexagons and the corresponding dashed lines, overlaid on the SDSS *gri* composite image, illustrate the locations from which the spectrum is extracted. In the case of low Gaussian amplitude over noise ratio (< 3) in emission lines, red labels are used. The format of the surrounding panels is the same as that of figure 2.

range of $n_{\rm e}$, in agreement with earlier theoretical works that predict the relationship between the kinetic energy released by the AGN and the energy required to induce the outflow ($\sim 0.1 - 5\%$, King (2005)). This is also consistent with the observational work of Tombesi et al. (2012), who showed that the typical ratios between the kinetic power of the outflows and the bolometric luminosities of 28 local AGNs are $\dot{E}_{\rm K}/L_{\rm bol} > 0.3\%$ for ultrafast outflows and $\sim 0.02\% < \dot{E}_{\rm K}/L_{\rm bol} < 0.8\%$ for non-ultrafast outflows. In figure 7, we present the kinetic power of the ionized gas (colored symbols, Brusa et al. (2015b); Carniani et al. (2015); Kakkad et al. (2016); Fiore et al. (2017); Toba et al. (2017); Davies et al. (2020); Santoro et al. (2020)) and molecular gas (empty black circles and plus symbols, Cicone et al. (2014); Fiore et al. (2017)), along with the measurement for Mrk 766 conducted in this work (red-filled stars). The data for Mrk 766 are well-aligned in terms of the coupling kinetic efficiencies ($\dot{E}_{\rm K}/L_{\rm bol}$) with other observed ionized gas outflows. This is somewhat lower than the theoretical predictions (King 2010; Zubovas & King 2012), which are about $\sim 5\%$ of ($\dot{E}_{\rm K}/L_{\rm bol}$). However, such a discrepancy can be interpreted as a natural consequence that our measurements of ($\dot{E}_{\rm K}/L_{\rm bol}$) likely trace only a small fraction of the total outflowing gas from Mrk 766.

Lastly, we compare the mass outflow rate in the form of ionized gas outflows with the accretion rate feeding the central AGN. The mass accretion rate can be expressed as follows,

$$\dot{m} = \frac{L_{\rm bol}}{\eta c^2} \, M_\odot \, {\rm yr}^{-1}, \tag{6}$$

where $L_{\rm bol}$ is the bolometric luminosity, η is the radiative efficiency, and c is the speed of light. We obtain a mass accretion rate of $\dot{m} \sim 0.01 \, M_\odot \, {\rm yr}^{-1}$, assuming $\eta = 0.1$, which is a typical value (e.g., Soltan (1982); Chokshi & Turner (1992); Yu & Tremaine (2002); Marconi et al. (2004); Cao & Li (2008); Ueda et al. (2014)) in a geometrically thin and optically thick standard accretion disc model. The mass outflow rate ($\dot{M}_{\rm out}$) we obtained is about 10 times larger ($n_{\rm e} = 1000 \, {\rm cm}^{-3}$), or about 300 times larger ($n_{\rm e} = 50 \, {\rm cm}^{-3}$), than the mass accretion rate ($\dot{m}$). Assuming that the mass outflow rate is constant across different physical scales, from sub-parsec to kilo-parsec, this implies that most of the mass is ejected in the form of ionized gas outflows, while only a minor fraction of the gas ($0.3\% - 10\%$) is involved in the accretion onto the SMBH (e.g., Izumi et al. (2023)).

3.4 Caveats

As discussed in Section 3.3, the mass, rate, and kinetic power of AGN-driven ionized gas outflows vary significantly depending on the choice of $n_{\rm e}$, which we did not attempt to constrain in this work. Given the current data obtained from the KOOLS-IFU observations and the complex nature of $n_{\rm e}$ as discussed in Davies et al. (2020), an investigation of realistic values for $n_{\rm e}$ is beyond the scope of this study.

Furthermore, the measured quantities ($M_{\rm out}$, $\dot{M}_{\rm out}$, and $\dot{E}_{\rm K}$) should be regarded as lower limits for the total outflowing gas, since the detected ionized gas component likely presents only a minor fraction of the total outflows across the host galaxy.

Additionally, we emphasize that we confirmed the existence of AGN-driven ionized gas outflows up to approximately 1 kpc from the center of the galaxy. This does not necessarily restrict the regions to which the outflow gas has reached, as the presented observational results are limited to the area covered by the KOOLS-IFU. Instead, it should be interpreted as our observation of powerful outflow gas traveling toward the outer regions of the host galaxy,
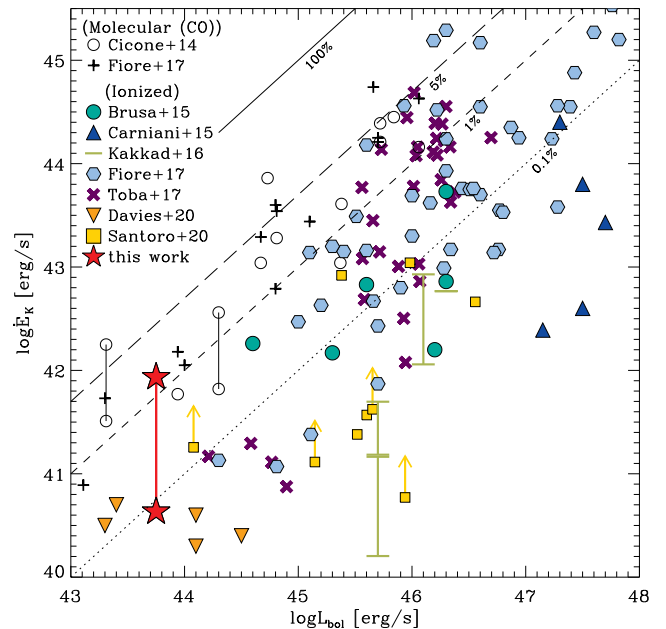

Fig. 7. Kinetic power of ionized gas outflow, $\dot{E}_{\rm K}$ vs. bolometric luminosity, $L_{\rm bol}$. The solid, long-dashed, dashed, and dotted lines represent the outflow kinetic power as 100%, 5%, 1%, and 0.1% of the AGN bolometric luminosity, respectively. Molecular outflows are presented by empty black circles and plus symbols (Cicone et al. 2014; Fiore et al. 2017)*, while the remaining colored data points correspond to ionized gas outflows (Brusa et al. 2015b; Carniani et al. 2015; Kakkad et al. 2016; Fiore et al. 2017; Toba et al. 2017; Davies et al. 2020; Santoro et al. 2020)*. The measurements of Mrk 766 in this work are presented as red-filled stars, with a range constrained by $n_{\rm e}$.

* Fiore et al. (2017) compiled the measurements from Downes & Solomon (1998); Tacconi et al. (1999); Lonsdale et al. (2003); Davies et al. (2004); Dasyra et al. (2006); Nesvadba et al. (2006); Davies et al. (2007); Nesvadba et al. (2008); Reyes et al. (2008); Veilleux et al. (2009); Engel et al. (2010); Howell et al. (2010); Harrison et al. (2012); Maiolino et al. (2012); Feruglio et al. (2013); Liu et al. (2013a, 2013b); Cicone et al. (2014); Genzel et al. (2014); Harrison et al. (2014); Sun et al. (2014); Brusa et al. (2015a, 2015b); Cicone et al. (2015); Cresci et al. (2015); Feruglio et al. (2015); Perna et al. (2015a, 2015b); Brusa et al. (2016); Kakkad et al. (2016); Wylezalek et al. (2016); Bischetti et al. (2017); Duras et al. (2017).

as captured by the KOOLS-IFU instrument, which has a limited field of view compared to the size of Mrk 766. Whether stronger outflows are moving at greater distances remains unknown, and further comprehensive observational studies are required to better constrain the properties of AGN-driven outflow gas.

4 Summary

We have presented optical IFU observations of innermost regions of Mrk 766, covering approximately 2 kpc × 2 kpc, using the KOOLS-IFU on the Okayama 3.8m Seimei telescope. Through multi-component spectral line fitting, we decomposed narrow emission lines as well as broad lines, detecting powerful outflowing gas in [OIII]λ5007 with velocities exceeding 500 km s^{-1}.

Non-parametric line width (W_{80}) and the asymmetry parameter (Δv) indicate that the central region of Mrk 766 is kinematically disturbed. We identified radially distributed strong AGN-driven outflows in the south-east and south-west, while the northern side from the center is weaker.

We estimated the mass of ionized outflowing gas to be $10^{4.65-5.95} M_\odot$, assuming an electron density in the range of 50 cm$^{-3} < n_e < 1000$ cm^{-3}. Under the same assumption, we estimated the outflow rate of ionized gas to be $0.14 - 2.73$ $M_\odot$yr^{-1}. We measured the kinetic power of the ionized outflow gas (4.31×10^{40} erg s$^{-1} < \dot{E}_K < 8.62 \times 10^{41}$ erg s^{-1}), which corresponds to a coupling efficiency of $0.08\% - 1.53\%$. The discrepancy between the observations and the theoretical predictions is likely a natural consequence of the fact that the observations used in this work trace only a small fraction of the total outflowing gas. The mass outflow rate in Mrk 766 is much larger ($10 - 300$ times) than the mass accretion rate, suggesting that at most 10% of the inflow is accreted by the SMBH, under the assumption that the mass outflow rate is constant across the different physical scales. Finally, we emphasize that the question of how far the outflowing gas has traveled remains uncertain.

References

Baldwin, J. A., Phillips, M. M., & Terlevich, R. 1981, PASP, 93, 5

Barden, S. C. & Armandroff, T., in S. C. Barden, ed., Fiber Optics in Astronomical Applications (1995), vol. 2476 of *Society of Photo-Optical Instrumentation Engineers (SPIE) Conference Series*, pp. 56–67

Barden, S. C., Armandroff, T., Muller, G., Rudeen, A. C., Lewis, J., & Groves, L., in D. L. Crawford & E. R. Craine, eds., Instrumentation in Astronomy VIII (1994), vol. 2198 of *Society of Photo-Optical Instrumentation Engineers (SPIE) Conference Series*, pp. 87–97

Barrows, R. S., Comerford, J. M., & Greene, J. E. 2018, ApJ, 869, 2, 154

Bellovary, J. M., Cleary, C. E., Munshi, F., Tremmel, M., Christensen, C. R., Brooks, A., & Quinn, T. R. 2019, MNRAS, 482, 3, 2913

Bentz, M. C. et al. 2009, ApJ, 705, 1, 199

Bischetti, M. et al. 2017, A&A, 598, A122

Bland-Hawthorn, J. et al. 2019, ApJ, 886, 1, 45

Blanton, M. R. et al. 2017, AJ, 154, 1, 28

Brusa, M. et al. 2015a, A&A, 578, A11

Brusa, M. et al. 2015b, MNRAS, 446, 3, 2394

Brusa, M. et al. 2016, A&A, 588, A58

Bruzual, G. & Charlot, S. 2003, MNRAS, 344, 4, 1000

Bundy, K. et al. 2015, ApJ, 798, 1, 7

Calzetti, D., Armus, L., Bohlin, R. C., Kinney, A. L., Koornneef, J., & Storchi-Bergmann, T. 2000, ApJ, 533, 2, 682

Cano-Díaz, M., Maiolino, R., Marconi, A., Netzer, H., Shemmer, O., & Cresci, G. 2012, A&A, 537, L8

Cano-Díaz, M. et al. 2022, AJ, 164, 4, 127

Cao, X. & Li, F. 2008, MNRAS, 390, 2, 561

Cappellari, M. & Emsellem, E. 2004, PASP, 116, 816, 138

Carniani, S. et al. 2015, A&A, 580, A102

Chambers, K. C. et al. 2016, arXiv e-prints, arXiv:1612.05560

Chokshi, A. & Turner, E. L. 1992, MNRAS, 259, 421

Cicone, C. et al. 2014, A&A, 562, A21

Cicone, C. et al. 2015, A&A, 574, A14

Comerford, J. M. & Greene, J. E. 2014, ApJ, 789, 2, 112

Cresci, G. et al. 2015, ApJ, 799, 1, 82

Dasyra, K. M. et al. 2006, ApJ, 651, 2, 835

Davies, R. et al. 2020, MNRAS, 498, 3, 4150

Davies, R. I., Müller Sánchez, F., Genzel, R., Tacconi, L. J., Hicks, E. K. S., Friedrich, S., & Sternberg, A. 2007, ApJ, 671, 2, 1388

Davies, R. I., Tacconi, L. J., & Genzel, R. 2004, ApJ, 613, 2, 781

Deconto-Machado, A. et al. 2022, A&A, 659, A131

Downes, D. & Solomon, P. M. 1998, ApJ, 507, 2, 615

Drory, N. et al. 2015, AJ, 149, 2, 77

Duras, F. et al. 2017, A&A, 604, A67

Engel, H. et al. 2010, A&A, 524, A56

Feruglio, C. et al. 2013, A&A, 549, A51

Feruglio, C. et al. 2015, A&A, 583, A99

Fiore, F. et al. 2017, A&A, 601, A143

Fischer, T. C., Crenshaw, D. M., Kraemer, S. B., & Schmitt, H. R. 2013, ApJS, 209, 1, 1

Gatto, L., Storchi-Bergmann, T., Riffel, R. A., Riffel, R., Rembold, S. B., Schimoia, J. S., Mallmann, N. D., & Ilha, G. S. 2024, MNRAS, 530, 3, 3059

Genzel, R. et al. 2014, ApJ, 796, 1, 7

Gonzalez Delgado, R. M. & Perez, E. 1996, MNRAS, 278, 3, 737

Harrison, C. M., Alexander, D. M., Mullaney, J. R., & Swinbank, A. M. 2014, MNRAS, 441, 4, 3306

Harrison, C. M. et al. 2012, MNRAS, 426, 2, 1073

Harrison, C. M. et al. 2016, MNRAS, 456, 2, 1195

Hoshi, A., Yamada, T., & Ohta, K. 2024, PASJ, 76, 1, 103

Howell, J. H. et al. 2010, ApJ, 715, 1, 572

Izumi, T. et al. 2023, Science, 382, 6670, 554

Kakkad, D. et al. 2016, A&A, 592, A148

Kakkad, D. et al. 2020, A&A, 642, A147

Kauffmann, G. et al. 2003, MNRAS, 346, 1055

Keel, W. C. et al. 2012, MNRAS, 420, 1, 878

Keel, W. C. et al. 2015, AJ, 149, 5, 155

Kewley, L. J., Dopita, M. A., Sutherland, R. S., Heisler, C. A., & Trevena, J. 2001, ApJ, 556, 121

Kewley, L. J., Groves, B., Kauffmann, G., & Heckman, T. 2006, MNRAS, 372, 961

King, A. 2005, ApJL, 635, 2, L121

King, A. R. 2010, MNRAS, 402, 3, 1516

Koss, M. et al. 2017, ApJ, 850, 1, 74

Koss, M. J. et al. 2022, ApJS, 261, 1, 2

Kukula, M. J., Pedlar, A., Baum, S. A., & O'Dea, C. P. 1995, MNRAS, 276, 4, 1262

Kurita, M. et al. 2020, PASJ, 72, 3, 48

Law, D. R. et al. 2015, AJ, 150, 1, 19

Liu, G., Zakamska, N. L., Greene, J. E., Nesvadba, N. P. H., & Liu, X. 2013a, MNRAS, 430, 3, 2327

Liu, G., Zakamska, N. L., Greene, J. E., Nesvadba, N. P. H., & Liu, X. 2013b, MNRAS, 436, 3, 2576

Lonsdale, C. J., Lonsdale, C. J., Smith, H. E., & Diamond, P. J. 2003, ApJ, 592, 2, 804

Maiolino, R. et al. 2012, MNRAS, 425, 1, L66

Marconi, A., Risaliti, G., Gilli, R., Hunt, L. K., Maiolino, R., & Salvati, M. 2004, MNRAS, 351, 1, 169

Markwardt, C. B., in D. A. Bohlender, D. Durand, & P. Dowler, eds., Astronomical Data Analysis Software and Systems XVIII (2009), vol. 411 of *Astronomical Society of the Pacific Conference Series*, p. 251

Matsubayashi, K. et al. 2019, PASJ, 71, 5, 102

McElroy, R., Croom, S. M., Pracy, M., Sharp, R., Ho, I. T., & Medling, A. M. 2015, MNRAS, 446, 2, 2186

McElroy, R. E. et al. 2016, A&A, 593, L8

Mejía-Restrepo, J. E. et al. 2022, ApJS, 261, 1, 5

Mezcua, M. & Domínguez Sánchez, H. 2020, ApJL, 898, 2, L30

Miller, L., Turner, T. J., Reeves, J. N., George, I. M., Kraemer, S. B., & Wingert, B. 2007, A&A, 463, 1, 131

Nagoshi, S., Iwamuro, F., Yamada, S., Ueda, Y., Oikawa, Y., Otsuka, M., Isogai, K., & Mineshige, S. 2024, MNRAS, 529, 1, 393

Namekata, K. et al. 2024, ApJ, 961, 1, 23

Nesvadba, N. P. H., Lehnert, M. D., De Breuck, C., Gilbert, A. M., & van Breugel, W. 2008, A&A, 491, 2, 407

Nesvadba, N. P. H., Lehnert, M. D., Eisenhauer, F., Gilbert, A., Tecza, M., & Abuter, R. 2006, ApJ, 650, 2, 693

Oh, K., Sarzi, M., Schawinski, K., & Yi, S. K. 2011, ApJS, 195, 13

Oh, K., Ueda, Y., Akiyama, M., Suh, H., Koss, M. J., Kashino, D., & Hasinger, G. 2019, ApJ, 880, 2, 112

Oh, K., Yi, S. K., Schawinski, K., Koss, M., Trakhtenbrot, B., & Soto, K. 2015, ApJS, 219, 1

Oh, K. et al. 2017, MNRAS, 464, 2, 1466

Oh, K. et al. 2018, ApJS, 235, 4

Oh, K. et al. 2022, ApJS, 261, 1, 4

Osterbrock, D. E. & Pogge, R. W. 1985, ApJ, 297, 166

Otsuka, M. 2022, MNRAS, 511, 4, 4774

Otsuka, M., Ueta, T., & Tajitsu, A. 2023, PASJ, 75, 6, 1280

Perna, M. et al. 2015a, A&A, 574, A82

Perna, M. et al. 2015b, A&A, 583, A72

Rey, S.-C., Oh, K., & Kim, S. 2021, ApJL, 917, 1, L9

Reyes, R. et al. 2008, AJ, 136, 6, 2373

Ricci, C. et al. 2017, ApJS, 233, 2, 17

Riffel, R. A. et al. 2023, MNRAS, 521, 2, 1832

Risaliti, G., Nardini, E., Salvati, M., Elvis, M., Fabbiano, G., Maiolino, R., Pietrini, P., & Torricelli-Ciamponi, G. 2011, MNRAS, 410, 2, 1027

Rodríguez-Ardila, A., Contini, M., & Viegas, S. M. 2005, MNRAS, 357, 1, 220

Rupke, D. S. N., Gültekin, K., & Veilleux, S. 2017, ApJ, 850, 1, 40

Sánchez-Blázquez, P. et al. 2006, MNRAS, 371, 2, 703

Santoro, F., Tadhunter, C., Baron, D., Morganti, R., & Holt, J. 2020, A&A, 644, A54

Sarzi, M. et al. 2006, MNRAS, 366, 1151

Schawinski, K., Koss, M., Berney, S., & Sartori, L. F. 2015, MNRAS, 451, 3, 2517

Schawinski, K., Thomas, D., Sarzi, M., Maraston, C., Kaviraj, S., Joo, S.-J., Yi, S. K., & Silk, J. 2007, MNRAS, 382, 1415

Schlegel, D. J., Finkbeiner, D. P., & Davis, M. 1998, ApJ, 500, 2, 525

Schönell, A. J., Riffel, R. A., Storchi-Bergmann, T., & Winge, C. 2014, MNRAS, 445, 1, 414

Shapovalova, A. I., Popović, L. Č., Burenkov, A. N., Chavushyan, V. H., Ilić, D., Kovačević, A., Bochkarev, N. G., & León-Tavares, J. 2010, A&A, 509, A106

Soltan, A. 1982, MNRAS, 200, 115

Sun, A.-L., Greene, J. E., Zakamska, N. L., & Nesvadba, N. P. H. 2014, ApJ, 790, 2, 160

Tacconi, L. J., Genzel, R., Tecza, M., Gallimore, J. F., Downes, D., & Scoville, N. Z. 1999, ApJ, 524, 2, 732

Taguchi, K. et al. 2023, ApJ, 958, 2, 156

Thacker, R. J., Scannapieco, E., & Couchman, H. M. P. 2006, ApJ, 653, 1, 86

Toba, Y., Bae, H.-J., Nagao, T., Woo, J.-H., Wang, W.-H., Wagner, A. Y., Sun, A.-L., & Chang, Y.-Y. 2017, ApJ, 850, 2, 140

Toba, Y. et al. 2022, PASJ, 74, 6, 1356

Toba, Y. et al. 2024, PASJ

Tody, D., in D. L. Crawford, ed., Instrumentation in astronomy VI (1986), vol. 627 of *Society of Photo-Optical Instrumentation Engineers (SPIE) Conference Series*, p. 733

Tody, D., in R. J. Hanisch, R. J. V. Brissenden, & J. Barnes, eds., Astronomical Data Analysis Software and Systems II (1993), vol. 52 of *Astronomical Society of the Pacific Conference Series*, p. 173

Tombesi, F., Cappi, M., Reeves, J. N., & Braito, V. 2012, MNRAS, 422, 1, L1

Ueda, Y., Akiyama, M., Hasinger, G., Miyaji, T., & Watson, M. G. 2014, ApJ, 786, 2, 104

Vasudevan, R. V., Mushotzky, R. F., Winter, L. M., & Fabian, A. C. 2009, MNRAS, 399, 1553

Vega Beltrán, J. C., Pizzella, A., Corsini, E. M., Funes, J. G., Zeilinger, W. W., Beckman, J. E., & Bertola, F. 2001, A&A, 374, 394

Veilleux, S., Rupke, D. S. N., & Swaters, R. 2009, ApJL, 700, 2, L149

Véron-Cetty, M. P. & Véron, P. 2010, A&A, 518, A10

Woo, J.-H. & Urry, C. M. 2002, ApJ, 579, 2, 530

Wylezalek, D., Flores, A. M., Zakamska, N. L., Greene, J. E., & Riffel, R. A. 2020, MNRAS, 492, 4, 4680

Wylezalek, D., Zakamska, N. L., Greene, J. E., Riffel, R. A., Drory, N., Andrews, B. H., Merloni, A., & Thomas, D. 2018, MNRAS, 474, 2, 1499

Wylezalek, D., Zakamska, N. L., Liu, G., & Obied, G. 2016, MNRAS, 457, 1, 745

Yamada, S. et al. 2024, ApJS, 274, 1, 8

Yan, R. et al. 2016, AJ, 152, 6, 197

Yu, Q. & Tremaine, S. 2002, MNRAS, 335, 4, 965

Zubovas, K. & King, A. R. 2012, MNRAS, 426, 4, 2751